AGU PUBLICATIONS

Water Resources Research

RESEARCH ARTICLE
10.1002/2015WR017555

Key Points:
- A time-scale hierarchy of physical and biological processes used to identify phytoplankton
- A general spatial distribution framework for phytoplankton concentration is developed
- The phytoplankton ecological niches are characterized

Correspondence to:
C. L. Marti,
marti1clelia@gmail.com

Citation:
Marti, C. L., J. Imberger, L. Garibaldi, and B. Leoni (2016), Using time scales to characterize phytoplankton assemblages in a deep subalpine lake during the thermal stratification period: Lake Iseo, Italy, *Water Resour. Res.*, *52*, 1762–1780, doi:10.1002/2015WR017555.

Received 14 MAY 2015
Accepted 26 DEC 2015
Accepted article online 30 DEC 2015
Published online 7 MAR 2016

Using time scales to characterize phytoplankton assemblages in a deep subalpine lake during the thermal stratification period: Lake Iseo, Italy

Clelia Luisa Marti[1], Jörg Imberger[2], Letizia Garibaldi[3], and Barbara Leoni[3]

[1]Centre for Water Research, University of Western Australia, Crawley, Western Australia, Australia, [2]Rosenstiel School of Marine & Atmospheric Science, University of Miami, Miami, USA, [3]Dipartimento di Scienze dell'Ambiente e del Territorio e di Scienze della Terra, Università degli Studi di Milano-Bicocca, Milano, Italy

Abstract A combination of field observations and 3-D hydrodynamic simulations were used to identify the phytoplankton species and to estimate the various time scales of the dominant physical and biological processes in Lake Iseo, a deep subalpine lake located in northern Italy, during a stratified period (July 2010). By ordering the rate processes time scales, we derive a phytoplankton patch categorization and growth interpretation that provides a general framework for the spatial distribution of phytoplankton concentration in Lake Iseo and illuminates the characteristics of their ecological niches. The results show that the diurnal surface layer was well mixed, received strong diurnal radiation, had low phosphorus concentrations and the phytoplankton biomass was sustained by the green alga *Sphaerocystis schroeterii*. The vertical mixing time scales were much shorter than horizontal mixing time scales causing a depth-uniform chlorophyll *a* concentration. The horizontal patch scale was determined by horizontal dispersion balancing the phytoplankton growth time scale, dictating the success of the observed green algae. The strongly stratified nutrient-rich metalimnion had mild light conditions and *Diatoma elongatum* and *Planktothrix rubescens* made up the largest proportions of the total phytoplankton biomass at the intermediate and deeper metalimnetic layers. The vertical transport time scales were much shorter than horizontal transport and vertical dispersion leading to growth niche for the observed phytoplankton. The study showed that time-scale hierarchy mandates the essential phytoplankton attributes or traits for success in a particular section of the water column and/or water body.

1. Introduction

The horizontal and vertical spatial variability of phytoplankton concentrations and their temporal succession have long been recognized as being of central ecological importance in the management of aquatic systems [e.g., *Denman and Gargett*, 1983; *Machado et al*., 2014; *Vidal et al*., 2014]. It is known that both the scales of the phytoplankton patches and the phytoplankton species succession are influenced by the time scales of the physical mixing processes at both the patch scale and the phytoplankton cell scales [e.g., *Kierstead and Slobodkin*, 1953; *Durham et al*., 2013; *Machado et al*., 2014]. The motion in the water column of a stratified lake experiences a great range of scales, all influencing the physical aspects of the phytoplankton habitat. The surface wind stress, the surface buoyancy fluxes, and the river inflows and outflows all act to disturb the stratified water column in the lake, inducing turbulence in the surface layer and generating a spectrum of internal waves, and so transferring the rate of working of these external forces to potential and kinetic energy of the internal waves. This store of potential and kinetic energy is then slowly released over the whole water column, at different scales, typically over days or weeks [*Saggio and Imberger*, 1998]. By supporting a spectrum of basin-scale internal waves, the stratification can accumulate and store the intermittent rate of external working introduced at the boundaries of the lake, then release it to the water column over a range of scales from the basin scale to the turbulent dissipation scale. In this way, the stratification of the water column plays a critical role for the phytoplankton population in a lake. Nutrients are recycled through the benthic boundary layer [*Nishri et al*., 2000; *Marti and Imberger*, 2006], shear driven instabilities in the metalimnion control phytoplankton resuspension [*McCabe and Cyr*, 2006], the heaving of the thermocline and the surface wave activity control the light climate in the biologically active surface layer

and metalimnion [*Evans et al*., 2008; *Hingsamer et al*., 2014] and the turbulence induced by wind directly at the water surface all influence phytoplankton succession [*George and Heaney*, 1978; *Cuypers et al*., 2011; *Machado et al*., 2014].

Machado et al. [2014] recently showed that patch scales and the biomass concentration of a phytoplankton bloom depend on the time scales of the vertical and horizontal mixing processes because within a patch an equilibrium state is reached between the biological growth rate and horizontal dispersion, as first hypothesized by *Kierstead and Slobodkin* [1953]. On the other hand, *Durham et al*. [2013] recently showed that phytoplankton succession is strongly dependent on water temperature, salinity, light availability, and nutrient levels at the cell scale, all being controlled in turn by the turbulence intensity. *Machado et al*. [2014] showed this control at the cell scale to be dependent on the ratio of the phytoplankton cell scale to the turbulent Batchelor length microscale, the length scale at which the rate of strain of the scalar concentration is balanced by molecular diffusion. If the cells are longer than the micro Batchelor nutrient scales, then they will experience nutrient maxima.

It is thus logical to ask whether the time scales imposed by the physical habitat control the selection of successful phytoplankton groups as well as of the patch characteristics in a stratified lake, and this is the objective of the present contribution. *Imberger* [1977] showed that the time-scale hierarchy of the rates of transport and mixing compared to the biological growth rates determines phytoplankton survival in lakes and reservoirs. Similar reasoning applies to the upper ocean [e.g., *Denman and Gargett*, 1983; *Denman and Powell*, 1984], to estuaries [e.g., *Atkinson et al*., 1987; *Koseff et al*., 1993; *Silva et al*., 2014] and to coral reefs [*Hatcher et al*., 1987], all pointing to the importance of physical time scales in determining/influencing the distribution of chemical and biological kinetics. The order of the time scales provides a framework for the interdependence of the interplay of the physical and biological processes.

The primary production in Lake Iseo, Italy, as in most lakes around the world, has seen a progressive increase due to increasing nutrient and organic matter loadings from the catchment [*Garibaldi et al*., 1999; *Schindler et al*., 2012; *Michalak et al*., 2013]. The increased primary production is leading to increased turbidity in the surface water, which in turn is adding to the water column stability, augmenting the stability increase due to global warming [*Verburg and Hecky*, 2009; *Gallina et al*., 2013; *Valerio et al*., 2015]. The implications of these changes are twofold. First, the water column stability increase is decreasing the frequency of lake overturn, reducing the thickness of the surface layer and thus reducing the living space for the resident fauna and flora. Second, the increased biological oxygen demand, triggered by the increased particulate flux into the hypolimnion, is causing a reduction of dissolved oxygen in the hypolimnion. Together, these two effects expose the lake's fauna and flora to the danger of total annihilation if a rapid overturn should occur during an exceptionally cold winter, simply because the increasing volume of the anoxic hypolimnion would overwhelm the small surface volume when mixing occurs [*Kling et al*., 1987; *Blenckner et al*., 2007; *Boehrer and Schultze*, 2008]. The water column stability of a lake, and thus the energy flux path, may be controlled with impellers [e.g., *Morillo et al*., 2009] and/or bubblers [e.g., *McDougall*, 1978] and so an understanding of how the physical habitat influences phytoplankton behavior is critical to the ecological management of deep lakes in the face of global warming and increased nutrient loading.

In this study, we present a combination of field observations and 3-D hydrodynamic simulations to identify the phytoplankton species and to estimate the various time scales of the dominant physical and biological processes in Lake Iseo during a period when the water column was stratified (July 2010). By ordering the rate time scales in a hierarchy, following that of *Imberger et al*. [1983], we derive a phytoplankton patch categorization and growth interpretation. This, in turn, allows the development of a general framework for the spatial distribution of phytoplankton concentration in Lake Iseo at the time of the field observations.

2. Methods

2.1. Physical and Biological Processes Time Scales

To understand the interplay of the physical and biological processes, a scaling analysis [e.g., *Imberger et al*., 1983; *Hatcher et al*., 1987; *Koseff et al*., 1993] was performed to identify the important nondimensional parameters controlling the phytoplankton groups and their distribution in Lake Iseo and so establish a general procedure for the categorization of the phytoplankton occurrences in stratified lakes in general.

Here we introduce terminology, definitions, and procedures used throughout the text to estimate the time scales of transport and mixing processes and phytoplankton growth, which place them in a single comparable currency. The subscripts SL, M, VM, HM, VT, HT, and I denote surface layer, metalimnion, vertical mixing, horizontal mixing, vertical transport, horizontal transport, and inflow, respectively. The time scale for vertical mixing in the vertically homogeneous, surface layer, $T_{SL;VM}$, is given by [*Imberger*, 1985]:

$$T_{SL;VM} = \frac{h}{u^*}, \tag{1}$$

where h is the depth of the diurnal surface layer and u^* is the wind induced water surface shear velocity calculated from $u^* = (C_d \rho_a / \rho_0)^{1/2} U$, where $C_d = 1.3 \times 10^{-3}$, is the assumed neutral water surface drag coefficient, $\rho_a = 1.2$ kg m^{-3}, is the air density, $\rho_0 = 1 \times 10^3$ kg m^{-3}, is the reference density for water and U is the wind speed at 10 m above the water surface. The time scale, $T_{SL;HM}$, for horizontal mixing in the surface layer of a patch with a characteristic length scale of size, L, [*Fischer et al*., 1979] may be expressed by:

$$T_{SL;HM} \sim \frac{L^2}{\kappa_{SL;HM}} \tag{2}$$

where $\kappa_{SL;HM} \sim u^* h$ is the horizontal dispersion coefficient in the surface layer. The time scale for vertical transport in the metalimnion, $T_{M;VT}$, [*Cuypers et al*., 2011; *Valerio et al*., 2012] is given by the period of the basin-scale internal wave modes induced by the wind and the time scale for the horizontal transport in the metalimnion can be expressed as $T_{M;HT} \sim \frac{L}{u}$, [*Marti and Imberger*, 2008], where u is the velocity scale induced by the internal mode in the metalimnion. The time scale for vertical mixing in the metalimnion, $T_{M;VM}$, [*Eckert et al*., 2002; *Yeates et al*., 2013] may be calculated from,

$$T_{M;VM} \sim \frac{h_M^2}{\kappa_{M;VM}} \tag{3}$$

where h_M is the metalimnion thickness scale [*Imberger*, 2013] and $\kappa_{M;VM}$ is the vertical diffusion coefficient in the metalimnion. The time scale for horizontal mixing in the metalimnion, $T_{M;HM}$, [*Eckert et al*., 2002] is given by

$$T_{M;HM} \sim \frac{L^2}{\kappa_{M;HM}} \tag{4}$$

where $\kappa_{M;HM}$ is the horizontal dispersion coefficient in the metalimnion. The time scale for inflow horizontal transport, $T_{I;HT}$, is controlled by the advective processes [*Hogg et al*., 2013]. Finally, τ_{SL} and τ_M are the growth time scales of dominant phytoplankton species in the surface layer and metalimnion, respectively, calculated as the reciprocal of phytoplankton specific growth rate [*Harris and Trimbee*, 1986; *Reynolds*, 2006].

These time scales were estimated based on field measurements and 3-D hydrodynamic simulations. As *Imberger* [1977] established, different systems may be classified into different flow regimes according to the time-scale ordering of the dominant processes. In terms of the processes of interest, i.e., advection, diffusion, and growth, we define a flow as "frozen" when the transport has the shortest time scale and the phytoplankton are simply advected by the water body, faster than they can grow or diffuse; as "diffusive" when mixing has the shortest time scale and any growth or patch distortion is immediately smoothed out by mixing faster than patches can form; and as "reactive" or "equilibrium" when growth has the shortest time scale [*Imberger et al*., 1983].

2.2. Study Site

Lake Iseo is a deep, subalpine, reverse-L-shaped lake, located in northern Italy (Figure 1). It is the fifth largest Italian lake in terms of volume, with a volume of 7.6 km^3, a surface area of 61.8 km^2, a maximum depth of 256 m, and a mean depth of 123 m. The major inflows into Lake Iseo are the Oglio River and the Industrial Canal at the northern end; the major outflow is the Oglio River at the southwestern end. The lake is narrow, with steep sides and a thalweg that is oriented approximately north-south. Monte Isola island, located in the central part of the lake, is the largest (surface area ~4 km^2) and highest (peak elevation ~420 m above the lake water surface) lacustrine island in Europe. The wind field, over the lake, is strongly influenced by the surrounding topography varying greatly spatially. This spatial variability is, in turn, imposed on the internal wave field within the lake [*Valerio et al*., 2012; *Vilhena et al*., 2013]. During summer 2010, the basin-scale internal wave modes, the surface manifestations of which most closely matched the wind spatial and temporal variability were excited most strongly. This match was predominantly with the 24.5 h fundamental-

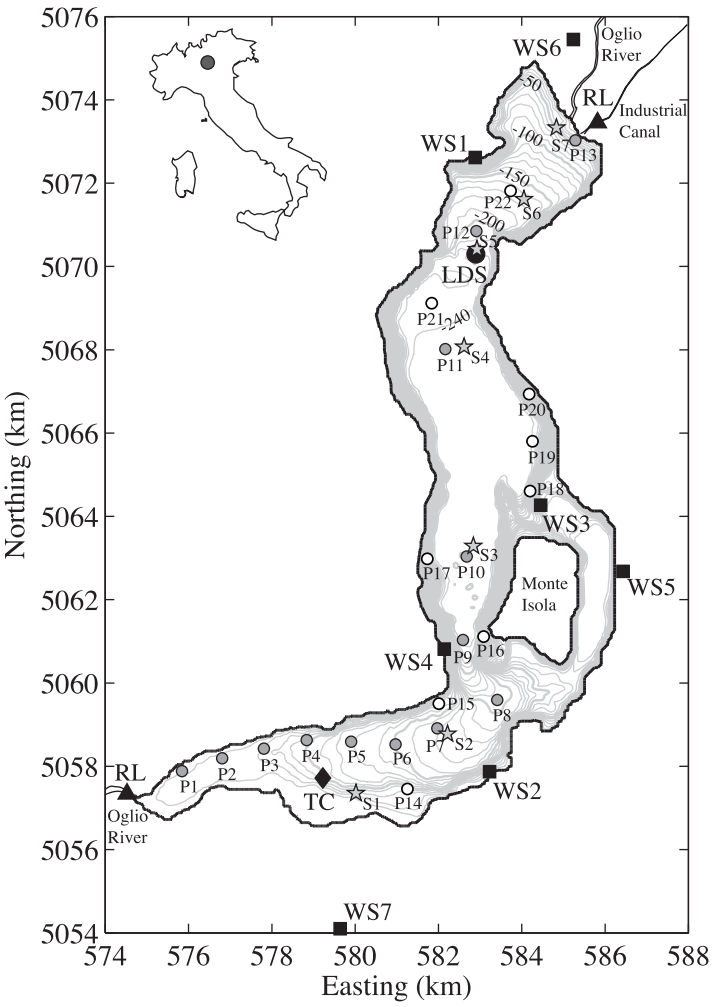

Figure 1. Location and bathymetry of Lake Iseo. The contour interval is 10 m. The circle and diamond indicate the locations of the Lake Diagnostic System (LDS) and the Thermistor Chain (TC), respectively, the squares indicate the location of the wind stations (WS) and the triangles the location of the river loggers (RL). Stars indicate the location of the water sampling sites (S1–S7) on 17 July 2010 and dots the location of the Multiple Scale Profiler (MSP) profiles on 15 July (P1–P13) and 17 July 2010 (P14–22), respectively.

mode V1H1 Kelvin wave rotating cyclonically around the basin. The higher vertical modes (V2H1) and locally higher horizontal modes (V1H5—a Poincaré-like wave trapped by Monte Isola) were also excited, but to a lesser extent [*Valerio et al.*, 2012]. Lake Iseo seasonally exhibits concentrations of cyanobacteria (mostly *Planktothrix rubescens*), green algae (mainly *Sphaerocystis schroeteri*), Conjugato-phyceae (mostly *Mougeotia* spp.), and diatoms (mainly *Fragilaria* sp. and *Diatoma elongatum*) [*Garibaldi et al.*, 2003; *Salmaso et al.*, 2003; *Leoni et al.*, 2014a]. Since the end of the 1980s, the deep layers of the lake have become deoxygenated and only two complete lake overturns have been observed in the last 20 years [*Leoni et al.*, 2014a].

2.3. Field Measurements

We used field data collected in Lake Iseo between 13 and 27 July 2010. A Lake Diagnostic System (LDS), a thermistor chain (TC), four wind stations (WS), and three river loggers (RL) were deployed and water sampling (S) was conducted as part of the experiment at locations shown in Figure 1. Water column profiles were taken with the boat-mounted, free-falling Multiple Scale Profiler (MSP).

2.3.1. Lake Diagnostic System (LDS)

The thermal structure in the northern part of the lake was continuously monitored, commencing in December 2009 with a LDS [*Imberger*, 1994] (Figure 1) consisting of a fast response, high precision, thermistor chain with 21 underwater sensors measuring water temperature at different depths, from 0.25 to 49.75 m below the surface. The LDS was also equipped with a full meteorological station, allowing simultaneous measurements of air temperature, relative humidity, wind speed, wind direction, incoming short wave radiation, and net total radiation, all 2.5 m above the water surface. The LDS sampling interval was set to 10 s.

2.3.2. Thermistor Chain (TC)

A thermistor chain with 18 underwater sensors, similar to those on the LDS, measuring water temperature at different depths between 1 m and 33 m below the surface, was installed in the southern part of the lake (Figure 1) to record the water temperature during the duration of the field experiment; the sampling interval was set to 10 s.

2.3.3. Wind Stations (WS)

Four wind stations were deployed around the lake shore during the experiment period to augment three existing land wind stations operated by government agencies (Figure 1). The stations used sampling intervals ranging between 30 s and 1 h.

2.3.4. Multiscale Profiler (MSP)

The MSP is a free-falling water-column profiler, based on the CWR F-probe [*Fozdar et al*., 1985; *Imberger*, 1994] and equipped with pressure, temperature, conductivity, pH, dissolved oxygen (DO), and photosynthetically active radiation (PAR) sensors. Also attached were a C6 Multi-Sensor Platform™ with six Cyclops-7™ submersible sensors (temperature, chlorophyll *a*, phycocyanin, phycoerythrin, Rhodamine dye, turbidity and colored dissolved organic matter) and a microstructure probe with pressure and fast temperature sensors. The MSP was deployed in free-fall mode with a fall velocity of about 0.15 m s^{-1}. A detailed description of the MSP is given in *Hogg et al*. [2013]. The MSP was used opportunistically over the experiment period, along longitudinal and cross transects, to investigate the spatial distribution of the above variables and their time variability (Figure 1). The GPS location of each profile was logged as part of the profile data file.

2.3.5. River Loggers (RL)

River loggers were installed at the two main inflows (Oglio River and Industrial Canal) and at the lake outlet (Oglio River) and set to sample at 5 min intervals (Figure 1). The logger in the Oglio River was installed on 23 June 2010 at a weir upstream from the river mouth, and was set to measure water level, temperature, and conductivity; the flow discharge was calculated using a simple rating curve obtained from the weir operating authority [*Hogg et al*., 2013]. A similar logger, with only a temperature sensor, was installed in the Industrial Canal on 18 June 2010; the conductivity was measured manually on three occasions during the field experiment and the flow discharge was available from the hydropower plant that controls the flow in the Industrial Canal. A full logger (water level, temperature and conductivity) was also installed at the lake's outlet for the duration of the field experiment. The Oglio River outflow rating curve was obtained from the Consorzio dell'Oglio.

2.3.6. Water Samples (S)

Nutrient concentrations, phytoplankton identification, and cell counts were obtained with water samples collected using a Van Dorn bottle on 17 July 2010 at the surface (0–1 m depth) and depths of 9–13 m and 15–19 m, at seven sites along the longitudinal axis of the lake (Figure 1). The sampling depths were varied slightly to correspond to the depths of peak chlorophyll *a* concentrations as recorded with the MSP. Two water samples were also collected in the Oglio and Industrial Canal inflows. For each water sample collected, a portion of the water sample (500 mL) was fixed with acetic Lugol's solution immediately after collection for laboratory phytoplankton counting and identification. The remaining water was stored in ice boxes for subsequent laboratory analysis of nutrients, including total phosphorus (TP), total nitrogen (TN), nitrate (NO_3), ammonium (NH_4), reactive phosphorus (PO_4), silica (SiO_2), and chlorophyll *a*. The nutrient analytical procedures followed standard methods [*APHA et al*., 1995] described in detail by *Garibaldi et al*. [2003]. Phytoplankton analysis was carried out on preserved subsamples and algal cells were counted on Zeiss Axiovert 135 and IM35 inverted microscopes. At least 200 individuals of the most abundant species were counted, with a counting error of $<$15% [*Lund et al*., 1958]. Mean algal cell volumes for each species were estimated using the approximation of cell morphology to regular geometric shapes [*Rott et al*., 2007]. Identification of species and definition of taxonomic orders followed the more recent monographs of the series Süßwasserflora von Mitteleuropa and specific manuals of the series Das Phytoplankton des Süßwassers (see *Leoni et al*. [2014b]).

2.3.7. Satellite Observations of Chlorophyll a

A set of 10 Medium-Resolution Imaging Spectrometer Full Resolution (MERIS FR) images of chlorophyll *a* with a pixel size of 300 m $\times$ 300 m, obtained from the European Space Agency (ESA), were used to gain lake-wide surface variation of chlorophyll *a* distribution during July 2010. Each of the images was captured around 10:00 h local time every 2–3 days. The satellite chlorophyll *a* data were acquired through the Satellite-based Information System on Coastal Areas and Lakes (SISCAL) service. Chlorophyll *a* concentrations were determined or measured by three techniques, with the MSP profiler via spectral response, by laboratory analysis of water samples and from satellite images. Figure 2 compares results by the three techniques.

2.4. Hydrodynamic Modeling

The Centre for Water Research hydrostatic version of the 3-D hydrodynamic Estuary, Lake, and Coastal Ocean Model (ELCOM) was used to quantify the time scales for the horizontal transport and mixing processes, $T_{SL;HM}$, $T_{M;VM}$, $T_{M;HM}$, $T_{M;HT}$, and $T_{I;HT}$, as these could not be estimated directly from field measurements. ELCOM is the most widely used and cited hydrodynamic model worldwide [*Trolle et al*., 2012] and has been successfully applied in numerous lakes and reservoirs [e.g., *Marti and Imberger*, 2008; *Morillo et al*., 2009;

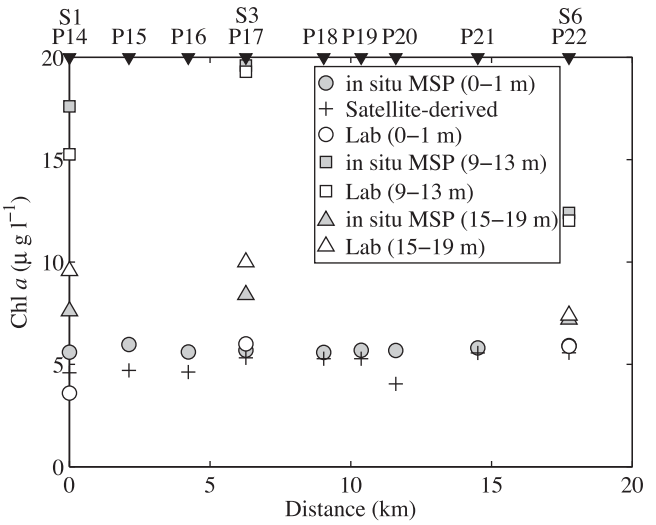

Figure 2. Comparison of different methods of measuring chlorophyll *a* concentrations: satellite-derived, determined in situ with the Multiple Scale Profiler (MSP) via spectral response (stations P14–P22 in Figure 1) and determined from laboratory analysis (water sampling sites S1, S3, and S6 in Figure 1) on 17 July 2010. (top) Water sampling and MSP station locations are indicated as arrows. The zero on the *x* axis is the location of station P14 shown in Figure 1.

Marti et al., 2011], including Lake Iseo [*Vilhena et al*., 2013; *Pilotti et al*., 2014b]. The governing equations and numerical schemes of ELCOM are described in detail in *Hodges et al*. [2000] and *Laval et al*. [2003].

The bathymetry of Lake Iseo was discretized using a uniform 80 m × 80 m horizontal grid. The vertical cell size ranged from 0.5 m for the upper 20 m, gradually expanding to 25 m for deep water. The simulations were performed for a period of 15 days, starting on 12 July, 00:00 h, with a time step of 30 s. They were initialized as a cold start with zero velocity at each grid cell and an initial water temperature distribution obtained by interpolating, both vertically and horizontally, the measured water temperature from the LDS and TC onto the numerical grid on 12 July at 00:00 h. A horizontally homogenous salinity field was used with an initial vertical structure obtained from a MSP salinity profile collected at the center of the lake on 15 July 2010. The atmospheric data (air temperature, relative humidity, shortwave radiation, and net total radiation), collected with the LDS and assumed uniform over the free surface of the model domain, were used to force ELCOM. The wind field was constructed, using a bilinear interpolation of measured wind data from the eight wind stations. A detailed explanation of the wind field construction may be found in *Valerio et al*. [2012]. The inflows from the Oglio River and the Industrial Canal and outflows from the Oglio River were used for the simulations [*Vilhena et al*., 2013]; the inflow temperatures, recorded by the river loggers, were used at the inflow boundary conditions. The Oglio River inflow salinity was obtained from the river logger (Figure 1) and the Industrial Canal inflow salinity was obtained from linear interpolation of spot measurements [*Hogg et al*., 2013].

Conservative numerical tracers were used in the model to assess the rate of horizontal dispersion centered at the seven water samples locations (see Figure 1). Each tracer was initially released at a concentration of unity, in grid cells at 2 m depth and 14 m depth in one model grid column, with a unique tracer at each location, producing instantaneous releases of equal loads of 10 tracers. Horizontal dispersion rates were derived following *Okubo* [1971] and *Lawrence et al*. [1995] using the horizontal area containing 90% of the tracer mass at time *t*. In addition, conservative tracers were continuously released with the inflows at a constant concentration of one. The rate of vertical turbulent diffusion during the time of the experiment was obtained by introducing two separate tracers, one as a lake-wide sheet, one cell thick, at 2 m in the surface layer and one in the metalimnion at 14 m depth, close to the 17°C isotherm on 13 July. The surface tracer was mixed down to a depth of about 7 m in 48 h, implying an average net vertical diffusion coefficient of around 2.8×10^{-4} m^2 s^{-1}.

3. Results

3.1. Observed and Simulated Thermal Structure and Response to the Wind Forcing

Wind forcing as measured at the LDS, and lake thermal structure measured at the LDS and TC locations, are shown in Figure 3. During the field experiment period, the wind exhibited a pronounced daily periodicity, characterized by northerly winds along the thalweg during the night and southerly winds during the afternoon (Figures 3a and 3b). During the field experiment period, two storm events were recorded at the LDS, the first during the early morning hours on 18 July with wind speeds reaching ~14 m s^{-1} and the second between 23 and 24 July with northerly wind speeds reaching ~10 m s^{-1} (Figures 3a and 3b). As seen in

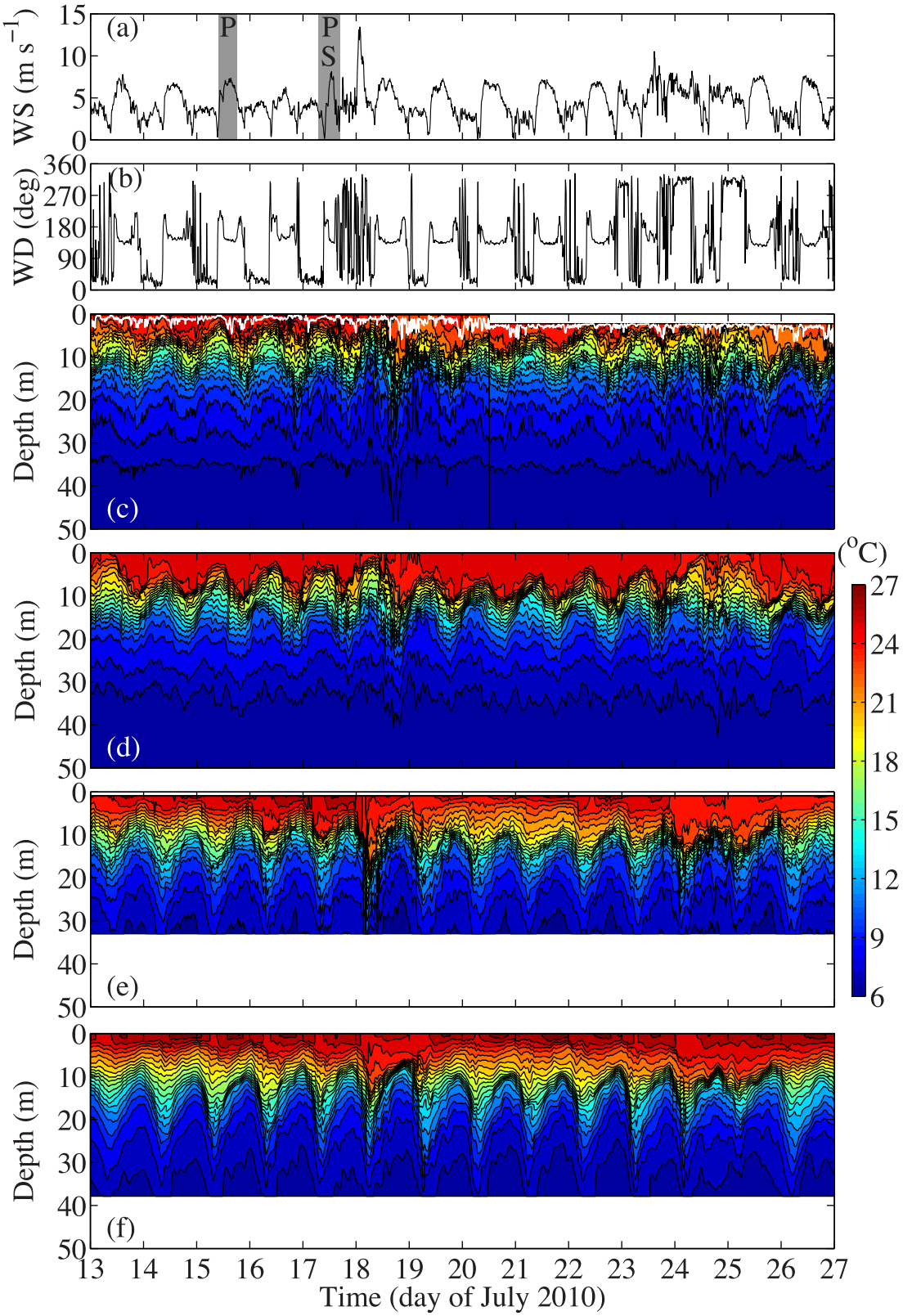

Figure 3. (a) Wind speed and (b) wind direction recorded by the Lake Diagnostic System (LDS); (c) water temperature recorded by LDS; (d) water temperature modeled by ELCOM at the LDS; (e) water temperature recorded by the Thermistor Chain (TC); and (f) water temperature modeled by ELCOM at the TC. The shaded areas in Figure 3a indicate the times of the Multiple Scale Profiler (MSP) profiles (P) on 15 and 17 July 2010 and water sampling (S) on 17 July 2010. In Figures 3c–3f, the bottom isotherm is 7°C and the contour interval is 1°C. The thick white line in Figure 3c indicates the depth of the diurnal mixed layer.

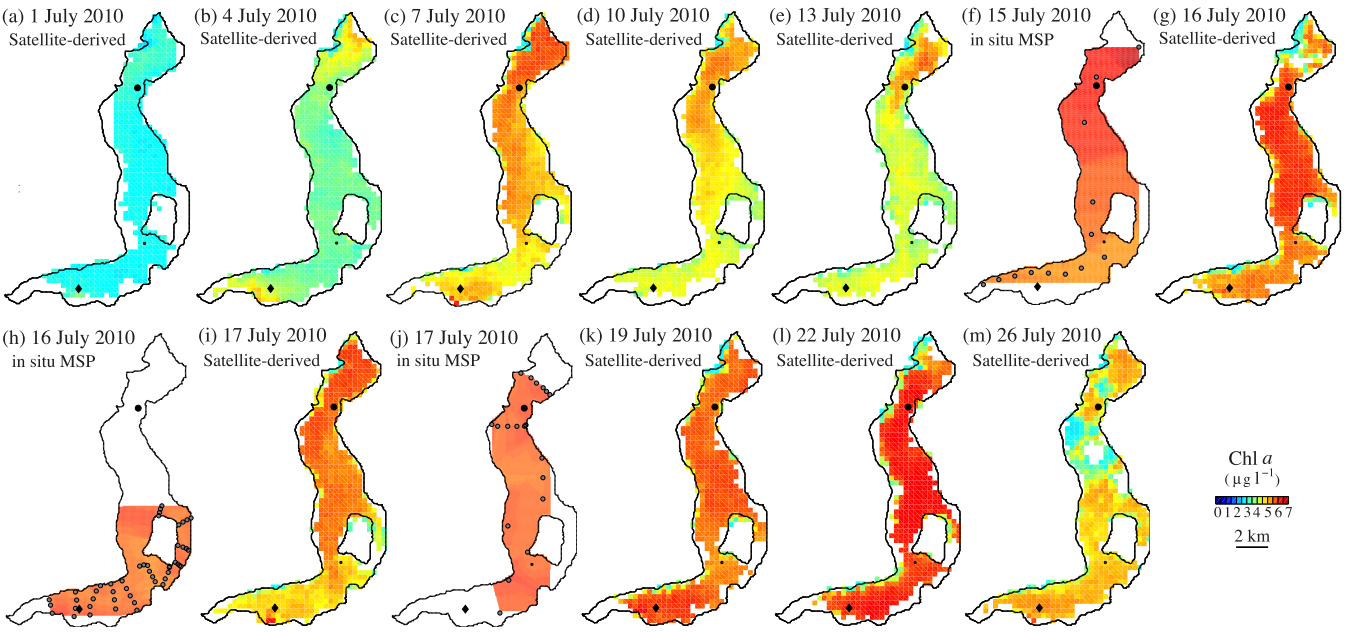

Figure 4. A time series of surface chlorophyll *a* concentrations in Lake Iseo in July 2010: (a–e, g, i, and k–m) satellite-derived and (f, h, and j) in situ Multiple Scale Profiler (MSP) profiles average of the surface 1 m. The location of the LDS and TC is shown in all plots. The location of the MSP profiles is shown in Figures 4f, 4h, and 4j.

Figures 3c and 3e, on average the water column exhibited a strong and relatively constant thermal stratification, with a warm (26°C) surface mixed layer separated from the cold hypolimnion (∼6.5°C) by a sharp metalimnion, ∼10 m thick. The surface water was generally slightly warmer at station TC (Figure 3e) in the southern basin compared to the surface water temperature at the LDS (Figure 3c), in the central and north basins.

The thermocline displacement revealed a pronounced 24.5 h periodicity (Figures 3c and 3e), associated with a V1H1 Kelvin wave rotating cyclonically around the basin [*Valerio et al.*, 2012]; the thermocline displacement recorded at the southern station, TC, was phase shifted by 180° relative to the displacements recorded by the LDS. The storm event on 18 July, induced a large depression of the metalimnion of about 15 m at TC and significant upwelling at the LDS, followed by a ca. 7.5 m downdraft. The closing of the metalimnion on 25 July followed by opening on 26 July at TC, with the opposite occurring at the LDS was identified by *Valerio et al.* [2012] as a result of the excitation of the higher vertical modes (V2H1) by the second storm event on 23 and 24 July.

The results from the ELCOM simulations were compared with the temperature records from the LDS and TC for the duration of the field experiment and are shown in Figures 3c–3f. The lake stratification and the phase and amplitude of isotherm displacements associated with the basin-scale interval waves were well reproduced by the model, including the wave response that followed the storm events of 18 July and 23–24 July, respectively. The main difference between the model and the field measurements was observed at LDS surface layer; the model consistently overmixed the top 5 m. The root mean square error (RMSE), a measure of the discrepancy between observations and simulations, calculated for the time series of depth of individual isotherms in Figures 3c–3f covering the simulation period was 0.89 m and 0.61 m at the LDS and TC respectively, providing confidence that the model results could be used for the estimation of the characteristic time scales required to establish the indicated time-scale hierarchy.

3.2. Observed Chlorophyll *a*, Dissolved Oxygen, pH, Nutrients, and Phytoplankton Distribution Patterns

The spatial and temporal distributions of the surface chlorophyll *a* concentration during the month of July obtained from the satellite images are shown in Figure 4. The concentration is seen to vary between 2.5 and 6.5 μg L^{-1} over space and time. For comparison, the chlorophyll *a* concentration derived from the MSP profiler (in situ fluorescence) averaged over the top 1 m is also included in Figure 4.

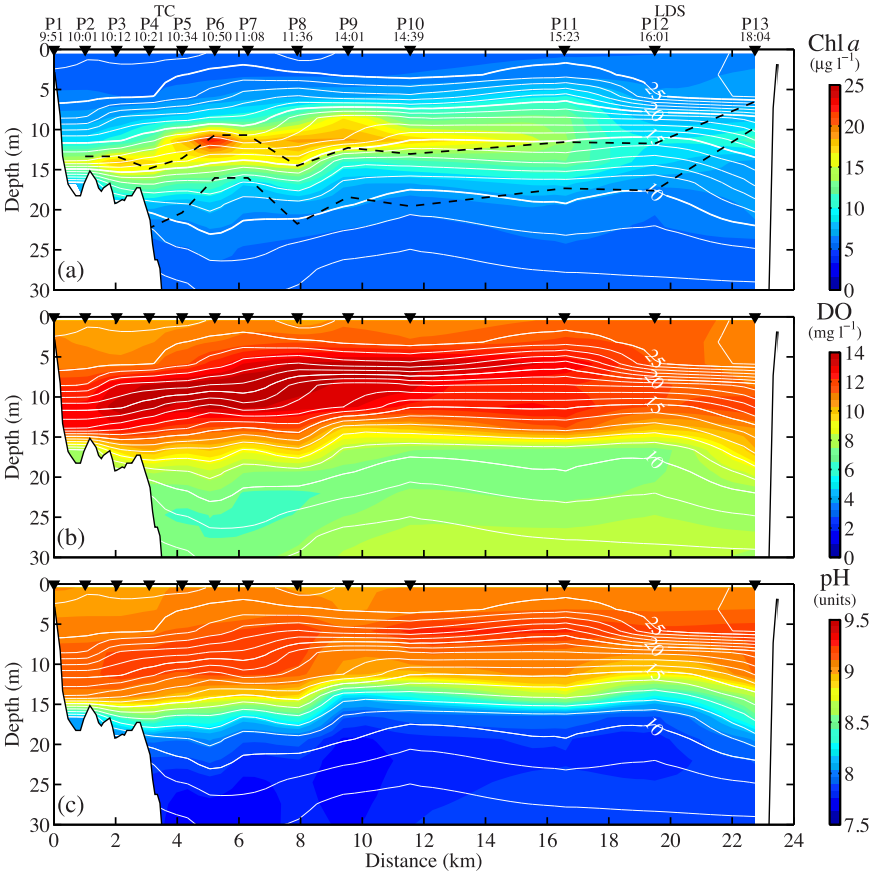

Figure 5. (a) Chlorophyll *a* concentration contours measured with the MSP (in situ fluorescence) along the south-north (transect) axis of the lake (see Figure 1, P1–P13) between 9:51 am and 6:04 pm on 15 July. (top) Profile station locations are indicated as arrows. Sampling times are indicated for all stations. Temperature contours are superimposed and shown as solid lines. The bottom isotherm is 8°C and the contour interval is 1°C. (b) Same as Figure 5a, but for dissolved oxygen. (c) Same as Figure 5a, but for pH. Black-dashed lines in Figure 5a mark the 1% and 0.1% of surface incident light derived from PAR measurements. The zero on the *x* axis is the location of station P1 shown in Figure 1.

A longitudinal MSP transect of vertical chlorophyll *a*, DO, and pH profiles measured along the south-north (transect) axis of the lake (see Figure 1) between 9:51 am and 5:52 pm on 15 July is shown in Figure 5 together with temperature contours. In the surface layer, chlorophyll *a* concentrations varied between 5 and 6 μg L^{-1}. Chlorophyll *a* concentrations reached maximum concentrations ranging from 12 μg L^{-1} at Site 13 to 24.5 μg L^{-1} at Site 6 in the metalimnion, indicating the existence of a pronounced deep chlorophyll maximum. The thickness and depth of the chlorophyll layer decreased from south to north; the depth of the chlorophyll maximum occurred at that corresponding to the 17°C isotherm ($z_{17°C}$) at most stations and sampling dates (Figures 5a and 6a). The close correlation between the upper and lower boundaries of the chlorophyll *a* patch and the depth of the 21°C ($z_{21°C}$) and 12 °C ($z_{12°C}$) isotherms, respectively, is evident in Figure 6b where chlorophyll *a* is plotted against the depth, normalized with respect to the thermal structure. Together these results indicate that the chlorophyll *a* concentration in the metalimnion is simply advected vertically up and down by the basin-scale internal wave seiching on time scales of a day or so. The corresponding DO concentrations and pH, shown in Figures 5b and 5c mirror the chlorophyll *a* behavior. Maximum DO and pH values (around 14 mg L^{-1} and 9.4, respectively) were measured in correspondence with high concentration of chlorophyll *a*.

Mean concentrations of nutrients and chlorophyll *a* obtained from the water samples collected along the south-north transect (Figure 1) between 10:50 am and 4:45 pm on 17 July are shown in Table 1. The nutrient concentrations varied widely in Lake Iseo between different depths, but only slightly horizontally between sampling sites. Inorganic N and its different forms increased progressively with depth while organic N, SiO_2, and PO_4 and TP showed maximum concentrations at depths of 9–13 m (the depth of 17°C isotherm). This

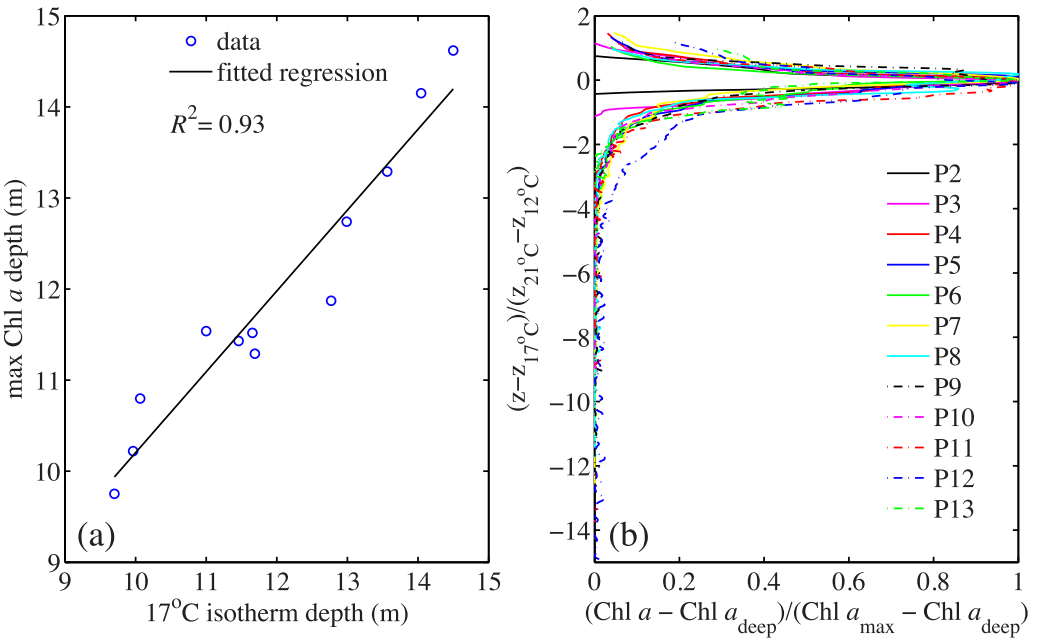

Figure 6. (a) Correlation between the depths of peak chlorophyll *a* concentration and the depths of the 17°C isotherm for the profiling data measured on 15 July 2010, and (b) normalized concentration of chlorophyll *a* against normalized depth.

pattern was also observed by *Leoni et al*. [2014b] using a Generalized Linear Model. Similarly, the total phytoplankton biomass and the taxa varied over depth, with less variation observed between the sampling sites along corresponding isotherms (see also *Leoni et al*. [2014b] and Figure 7).

Four taxa, *Diatoma elongatum*, *Planktothrix rubescens*, *Mougeotia* sp., and *Sphaerocystis schroeteri* accounted for more than 90% of the total biovolume of the identified taxa. Phytoplankton biomass peaked at all sampling sites at the depth of the 17°C isotherm (Figures 5a and 7a). In the surface layer, phytoplankton biomass consisted of the green alga *Sphaerocystis schroeterii* that contributed 55.5% of the biovolume of the identified taxa (Figure 7b); this is the species visible in the satellite images (Figure 4). At the intermediate and deeper metalimnetic layers, cyanobacteria and diatoms made up the largest proportions of the total phytoplankton biomass. In the intermediate metalimnetic layer, between 9 and 13 m, *Planktothrix rubescens* and *Diatoma elongatum* contributed 32% and 37% of the total biovolume, respectively. High levels of *Diatoma elongatum* were found at S2 and S3 whereas high levels of *Planktothrix rubescens* were found at S4, S5, and S6 (Figures 7c and 7d). In the deeper metalimnetic layer, between 15 and 19 m, *Planktothrix rubescens* and *Diatoma elongatum* contributed 24% and 40% of the total biovolume. High levels of *Diatoma elongatum* and of *Planktothrix rubescens* were found at S2 (Figure 7d). The corresponding mean ecological drivers of the dominant phytoplankton taxa for growth such as light, temperature, nutrients, and motility are detailed in Table 2.

Table 1. Mean Values (M) and Standard Deviations (SD) of Chlorophyll *a* (Chl *a*), Total Phosphorus (TP), Reactive Phosphorus (PO_4), Total Nitrogen (TN), Inorganic Nitrogen (InN), Nitrate (NO_3), Ammonium (NH_4), Organic Nitrogen (OrN), and Silica (SiO_2) of the Water Samples Taken in Lake Iseo on 17 July 2010 at the Three Different Depths[a]

Variable Depth		Chl *a* (μg L^{-1})	TP (μg L^{-1})	PO_4 (μg L^{-1})	TN (μg l^{-1})	InN (μg L^{-1})	NO_3 (μg L^{-1})	NH_4 (μg L^{-1})	OrN (μg L^{-1})	SiO_2 (μg L^{-1})
1 m	M	5.49	11.00	5.14	783.3	391.30	361.40	29.86	392.00	731.90
	SD	0.99	0.82	0.90	96.62	41.05	28.54	22.00	77.82	68.04
9–13 m	M	15.96	21.57	10.14	1166.00	542.40	495.70	46.71	623.70	932.30
	SD	5.64	3.51	1.77	160.90	34.38	26.37	11.24	141.40	235.10
15–19 m	M	7.50	17.43	5.14	1187.00	750.60	694.30	56.29	436.60	701.60
	SD	2.65	3.36	0.69	102.10	68.78	80.39	16.97	47.00	55.15

[a]The mean values were calculated from the seven stations.

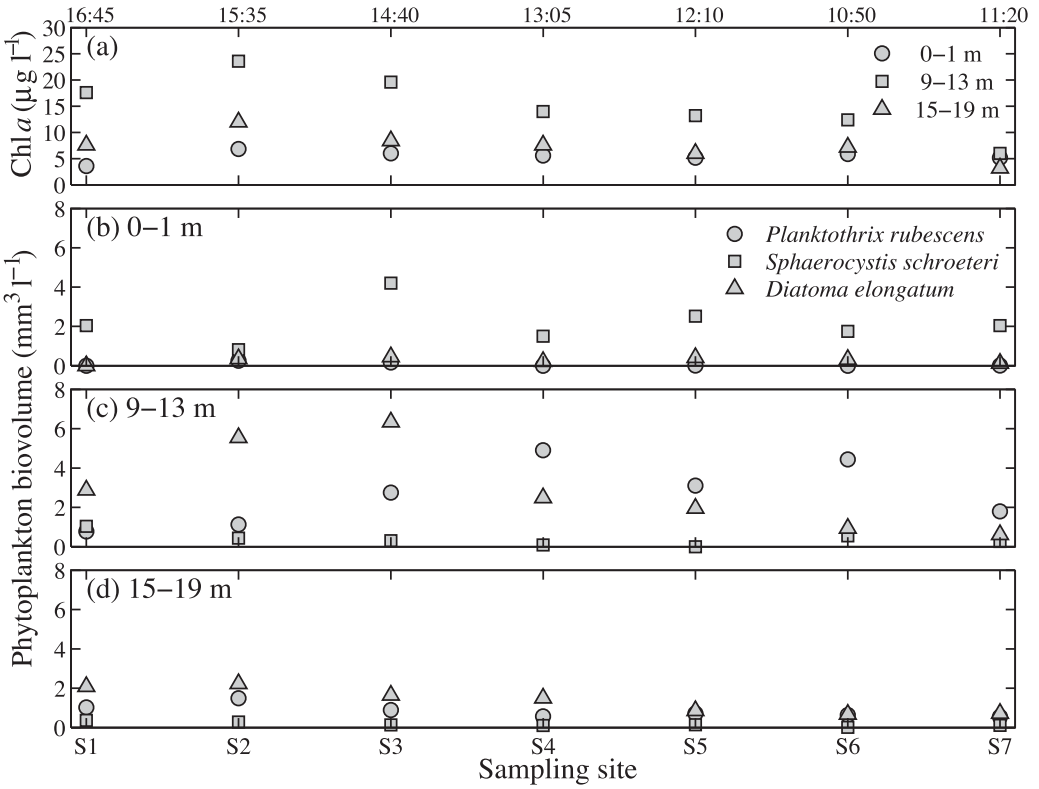

Figure 7. (a) Chlorophyll *a* concentrations at different depth of the water sampling sites; (b–d) phytoplankton biovolume at the different depths of the sampling sites on 17 July 2010 (see Figure 1).

4. Discussion

We now use field observations and 3-D hydrodynamics simulations to determine and establish a time-scale hierarchy of the transport and mixing processes and phytoplankton growth. The ordering of the time scales is the used to develop a general framework for the spatial distribution of phytoplankton concentration in Lake Iseo at the time of the field observations that allows the characterization of their ecological niches.

Table 2. Properties of Dominant Algal Species Making Up Observed Chlorophyll *a* Concentration

Group and Depth Observed	Species	Light Lim	Temp Lim	N Lim	P Lim	In Situ Growth (days)	Motility
Green 1 m	*Sphaerocystis schroeterii*[a,b]	High light	26°C	Low	Low	1.4–2.2	Immotile specie. Gelatinous sheath as a mechanism for reducing sinking rates.
Cyanobacteria 9–13 m 15–19 m	*Planktothrix rubescens*[a,c,d]	Low light	10–20°C	Low	Low	1.0–8.0	Gas vesicles that allow for positive buoyancy to accumulate within the depth of optimal irradiance. The resistance of gas vesicles to hydrostatic pressures is critical for the survival in deep lakes.
Diatom 9–13 m 15–19 m	*Diatoma elongatum*[a,e,f]	Low light	Need low temp 18°C	Low	Low	0.8–1.5	Neutrally buoyant at 18°C. Population increased with stronger water movement.

Temp = water temperature; N = nitrogen; P = phosphorus; Lim = limitation.
[a] *Reynolds* [2006].
[b] *Kampe et al.* [2007].
[c] *Bright and Walsby* [2000].
[d] *Oberhaus et al.* [2007].
[e] *Busse and Snoeijs* [2003].
[f] *Garibaldi et al.* [2003].

4.1. Surface Layer

In the diurnal surface mixed layer, defined by the layer of uniform temperature (temperature change less than 0.075°C, see Figure 3c), the chlorophyll *a* concentration increased by growth, the rate being determined by the nutrient concentration, the water temperature, the light intensity, and the turbulence intensity [*Machado et al*., 2014] and increased when the surface layer deepened into the metalimnion, as the concentration below the base of the surface layer was higher than that in the surface layer (see Figure 5a) and decreased when diluted by horizontal dispersion. This maybe expressed mathematically [*Kierstead and Slobodkin*, 1953] by:

$$\frac{\partial C_m(x_1,x_2,t)}{\partial t}=\kappa_1\frac{\partial^2 C_m(x_1,x_2,t)}{\partial x_1^2}+\kappa_2\frac{\partial^2 C_m(x_1,x_2,t)}{\partial x_2^2}+\frac{\Delta C_m(x_1,x_2,t)}{h}\frac{\partial h}{\partial t}+\alpha C_m(x_1,x_2,t) \tag{5}$$

where C_m is the chlorophyll *a* concentration, t is time, x_i is the coordinate in the ith direction, κ_i is the eddy diffusivity in the ith direction, and α is the growth rate for the resident conditions in the homogeneous diurnal surface layer of depth h.

From Figure 5a, it is seen that within the diurnal surface layer, above the 25°C isotherm, chlorophyll *a* was also uniform, but below the base of the diurnal surface layer the chlorophyll *a* concentration generally increased with depth. The homogeneity of chlorophyll *a* in the surface layer may be explained by comparing the vertical mixing time scale, $T_{SL;VM}$, with the growth time scale, τ_{SL}. For the LDS location, substituting values from Figures 3a and 3c into equation (1) leads to the time scale $T_{SL;VM}$ ranging from 50 to 400 s (∼1–7 min).

The growth time scale in the surface layer, τ_{SL}, may be estimated from the transition from 1 July to 7 July (Figures 4a–4c), a 6 day period when the winds were generally less than 4 m s^{-1} (not shown) [*Pilotti et al*., 2013] with little or no surface layer deepening and where the chlorophyll *a* concentration increased from about 3 μg L^{-1} on 1 July to 4 μg L^{-1} on 4 July and to 5.5 μg L^{-1} on 7 July. Given that the chlorophyll *a* concentration was relatively uniform across the whole lake (see Figures 4a–4c), it may be assumed that growth is independent of horizontal dispersion so that equation (5) reduces to:

$$\frac{dC_m(t)}{dt}=\alpha C_m(t) \tag{6}$$

Matching the solution of equation (6) to the growth rate shown in Figure 4, leads to:

$$C_m=3.0\,e^{0.10t} \tag{7}$$

where the growth rate and the factor 3 were determined from the initial concentration value at $t=0$ and the final value at $t=6$ (days). Using equation (7) at $t=3$ the predicted value is 4.06 μg L^{-1}, indicating the exponential growth model with a growth time scale of 10 days provides a good approximation to the observations [*Reynolds*, 2006].

Clearly, the vertical mixing time scales were much shorter than the growth time scale of the resident phytoplankton in the surface layer (*Sphaerocystis schroeteri*) so the flow may be described as vertically diffusive implying a depth-uniform chlorophyll *a* concentration in the surface layer; this was confirmed by the MSP data as seen in Figure 5a (above the 25°C) and implies that, in general, the chlorophyll *a* concentration in the homogeneous surface layer, may be written in the form:

$$C(x_1,x_2,x_3,t)=C_m(x_1,x_2,t)+\Delta C(x_1,x_2,x_3,t)H(-x_3-h(t)), \tag{8}$$

where $\Delta C(x_1,x_2,x_3,t)$ is the concentration jump at the base of the surface layer, $H(-x_3-h(t))$ is the Heaviside step function [*Fischer et al*., 1979], and $C_m(x_1,x_2,t)$ is the concentration in the surface layer that may be obtained by integrating equation (5) over the depth:

$$\frac{\partial C_m(x_1,x_2,t)}{\partial t}=\kappa\left(\frac{\partial^2 C_m(x_1,x_2,t)}{\partial x_1^2}+\frac{\partial^2 C_m(x_1,x_2,t)}{\partial x_2^2}\right)+\frac{\Delta C_m(x_1,x_2,x_3,t)}{h}\frac{\partial h}{\partial t}+\alpha C_m(x_1,x_2,t) \tag{9}$$

From equation (9), it is seen that the chlorophyll *a* concentration is governed by the rate of growth $\alpha=0.10$, the rate of entrainment at the base of the diurnal surface layer, and the rate of horizontal dispersion. As seen from Figure 7, the phytoplankton species composition was not uniform in space implying that vertical mixing was spatially variable, entraining the higher chlorophyll *a* concentration at depth into the

surface layer at locations where the diurnal surface layer deepening was most severe. However, at these locations it would also be expected to see in the surface layer higher concentrations of the metalimnetic phytoplankton species, *Planktothrix rubescens* and *Diatoma elongatum*. Inspection of the results in Figure 7b would suggest minimum deepening occurred at stations S1 and S2 on or before 17 July (southern reaches of Lake Iseo, see Figure 3e), and accentuated deepening in the northern reaches of Lake Iseo, starting at S3. This was reflected in the LDS measurements (Figure 3c) that show a surface layer deepening from 2 m to about 5 m at the LDS on 15 and 16 July for an extended period of nearly 12 h. From equation (9), it is seen that such differential deepening would have increased the chlorophyll *a* concentrations at S3 by:

$$\delta C_m(x_1, x_2, t) = + \frac{\Delta C_m(x_1, x_2, t)}{h} \delta h \tag{10}$$

The horizontal patch scale of the surface chlorophyll *a* concentrations, shown in Figure 4, had a longitudinal scale of around 3 to 5 km, slightly larger than the average width of the lake. If it is assumed that the entrainment at the base of the surface layer does not impose a separate length scale, and that the concentration is well mixed across the width of the lake, then the concentration may be modeled by:

$$\frac{\partial C_m(x_1, t)}{\partial t} = \kappa \frac{\partial^2 C_m(x_1, t)}{\partial x_1^2} + \alpha C_m(x_1, x_2, t) \tag{11}$$

where x_1 is the longitudinal coordinate. *Kierstead and Slobodkin* [1953] showed that a solution to equation (11) is given by:

$$C_m(x_1, t) = e^{\alpha t} f\left(\frac{x_1}{(\kappa t)^{\frac{1}{2}}}\right), \tag{12}$$

the patch growth process governed by growth balancing horizontal dispersion. The expected horizontal scale of a phytoplankton patch in the surface layer, L_P, is thus given by:

$$L_P \sim 4(\kappa_{SL;HM} \tau_{SL})^{\frac{1}{2}}, \tag{13}$$

where $\kappa_{SL;HM}$ is the horizontal dispersion coefficient in the diurnal surface layer.

Lake Iseo is oriented approximately north-south, with the wind over the lake being channeled by the mountains along the thalweg of the lake (Figures 3a and 3b) and the horizontal water currents in the surface layer were predominantly aligned in the south-north direction with a period of approximately 24 h [*Valerio et al*., 2012]. Progressive aerial distribution of the numerical tracers at 1, 3, and 6 days after release at 00:00 h on 13 July, at 2 m below the water surface and the 6 day average horizontal dispersion rates for each patch are presented in Figures 8a–8g. The horizontal dispersion coefficient, $\kappa_{SL;HM}$, averaged over the 6 days, ranged from 1.5 $m^2\ s^{-1}$ in the southern basin, to 11.7 $m^2\ s^{-1}$ in the central basin near Monte Isola and 5 $m^2\ s^{-1}$ near P11, the center of the surface chlorophyll *a* max (Figure 5a). Substituting these values into equation (13) results in a horizontal patch scale for the surface manifestations of the phytoplankton of around ~4 km, comparing well with the scale observed from the satellite chlorophyll *a* measurements (Figure 4). It should be noted that surface tracer extended vertically to the depth of the 20°C isotherm, deeper than the diurnal surface layer (Figure 9a).

The surface layer chlorophyll *a* concentration may thus be explained by the growth time scale of around 2 days (Table 2) and two wind events mixing the surface layer, increasing the surface chlorophyll *a* concentration with chlorophyll from depth, and a horizontal patch scale that is determined by the horizontal dispersion coefficient in the diurnal surface layer, leading to a time-scale hierarchy:

$$\frac{T_{SL;VM}}{\tau_{SL}} < \frac{T_{SL;HM}}{\tau_{SL}} \sim 1 \tag{14}$$

In the surface layer, the phytoplankton biomass was sustained by the green alga *Sphaerocystis schroeterii*. This species is immotile and has low nutrient requirements [*Reynolds*, 2006; *Kampe et al*., 2007] (see Table 2) tending to saturate growth at higher irradiance than other microalgal classes and thus tolerating high light radiation levels [*Richardson et al*., 1983]. During the study period, the surface water received strong diurnal radiation and had low phosphorus concentrations (~11 $\mu g\ L^{-1}$, Table 1), forming a favorable environment for *Sphaerocystis schroeterii* to dominate in the turbulent, well-mixed surface layer. The time-scale hierarchy

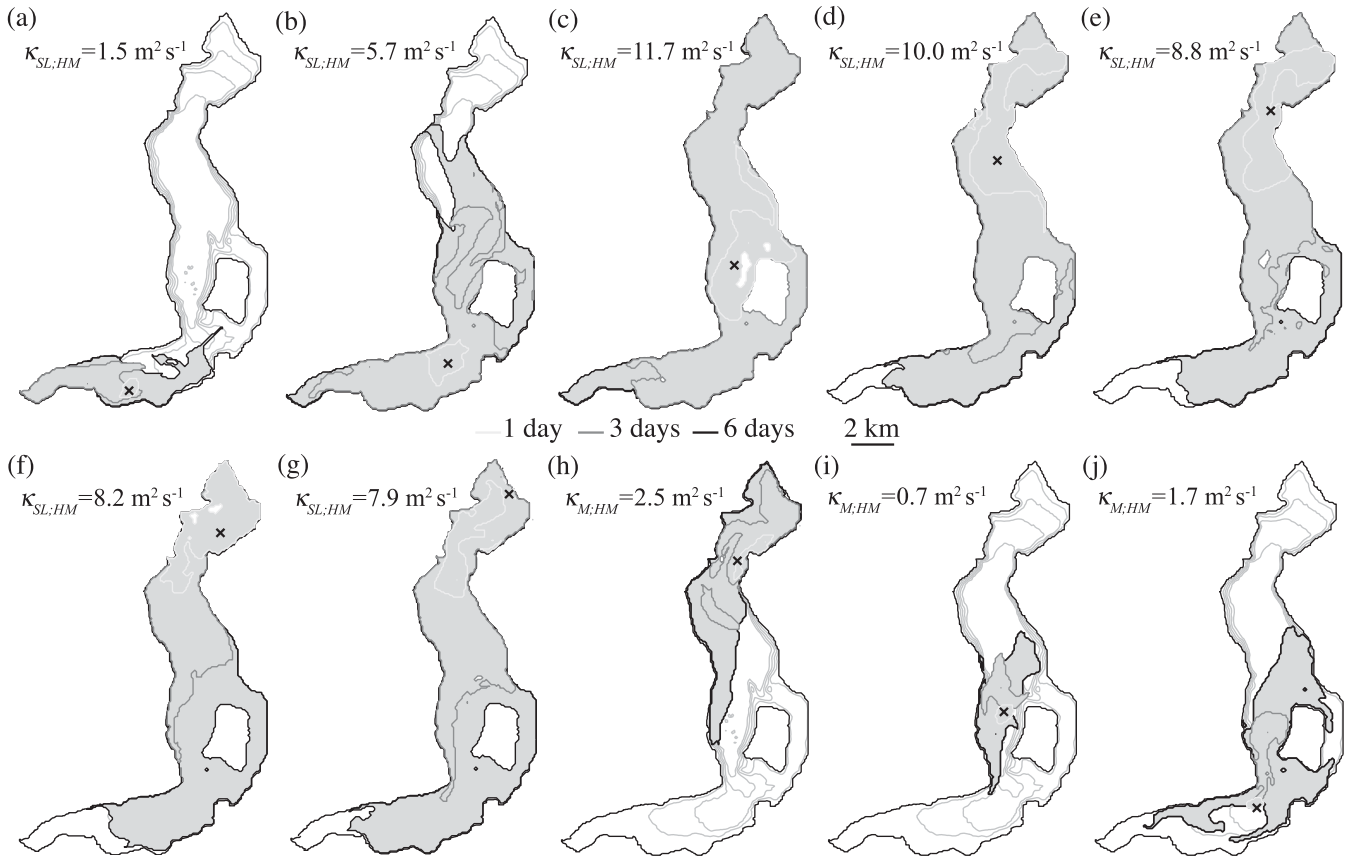

Figure 8. Progressive areal distribution of 90% of the tracer mass at 1, 3, and 6 days after release at 00:00 h on 13 July 2010 at (a)–(g) 2 m below the surface and (h)–(j) 14 m depth. Crosses mark release location. The 6 day average horizontal dispersion rates for each patch are presented.

suggests that green algae should be expected in the diurnal surface layer, well mixed vertically, but forming patches with a typical scale of around 3 ∼5 km. These predictions are confirmed, as seen from Table 2.

4.2. Metalimnion

The strong stratification defining the metalimnion and the associated basin-scale internal waves [*Cuypers et al.*, 2011; *Valerio et al.*, 2012; *Hingsamer et al.*, 2014] are significant for the phytoplankton residing in the metalimnion. To test the frozen flow nature of the metalimnion biology, the depth of the peak chlorophyll *a* concentration of each profile (Figure 5a) was plotted against the depth of the 17°C isotherm (Figure 6a); clearly the peak chlorophyll *a* concentration moved up and down with the water that is heaving up and down in response to the V1H1 basin-scale internal wave. Also observable from Figures 5a and 6a is a slight broadening of the chlorophyll *a* concentration centered on profiles P10 and P12 in what appears as the response to the V2H1 basin-scale internal wave mode. The response to this mode pulsing was tested by plotting, as shown in Figure 6b, the normalized chlorophyll *a* concentration against the depth normalized by the metalimnion thickness. It can be seen that the chlorophyll *a* concentration profiles collapsed on to one curve, indicating that the transport and possible mixing that influence the temperature profiles equally influenced the chlorophyll *a* concentrations.

The strong stratification at the level of the thermocline inhibited vertical mixing (Figures 3c, 3e, and 9). The horizontal and vertical eddy down-gradient diffusion coefficients for these strongly stratified metalimnetic shear flows [*Yeates et al.*, 2013] were also estimated by inserting a set of tracers in one grid cell at three locations at a depth of the thermocline and using the simulations to track their rate of spread, horizontally (Figures 8h–8j) and vertically (Figure 9b). From the rates of spread, the horizontal diffusion coefficient varied from 0.9 m^2 s^{-1} for the tracer release near Monte Isola to 1.7 and 2.5 m^2 s^{-1} for the tracers released in the south and north of the lake, respectively (Figures 8h–8j), while the vertical diffusion coefficient, $\kappa_{M;VM}$, was around 10^{-6} m^2 s^{-1} (Figure 9b), the same order of magnitude as those estimated from microstructure

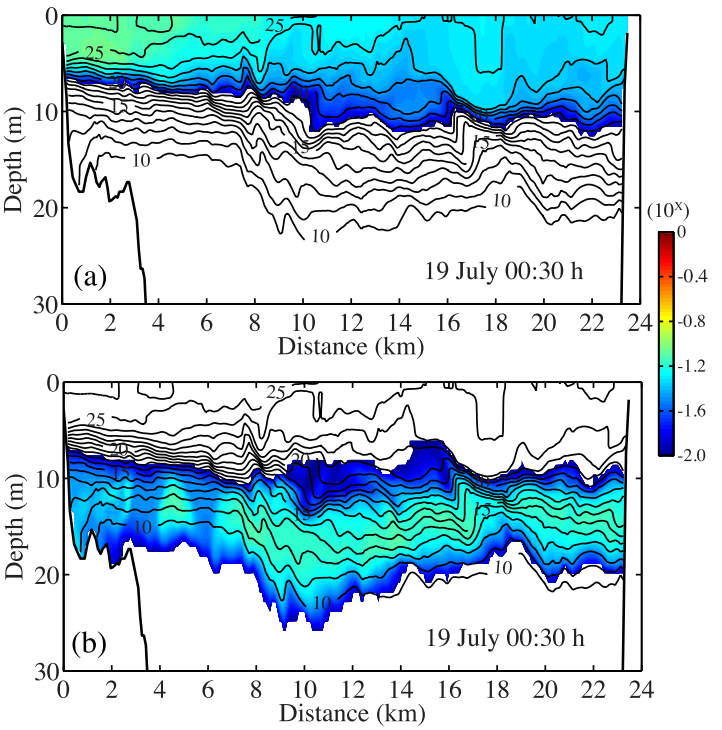

Figure 9. Distribution of the tracer released as a lake wide sheet at (a) 2 m and (b) at 14 m below the surface, respectively, along the longitudinal axis (south-north) of the lake after 6 days. Simulated temperature contours are superimposed and shown as solid lines. The bottom isotherm is 10°C and the contour interval is 1°C.

measurements (not shown). If we consider the metalimnion thickness scale for the fundamental solution of the diffusion equation [*Imberger*, 2013], $h_M = (z_{21°C} - z_{12°C})/4 = 2$ m, and substitute these values into equation (3) leads to a $T_{M;VM}$ value of around 46 days. This implies that any phytoplankton group resident in the metalimnion must be neutrally buoyant; negatively buoyant algae would sink out.

Valerio et al. [2012] and *Vilhena et al*. [2013] characterized the basin-scale internal wave modes in Lake Iseo and their response to wind stress. The storm passage on 18 July generated a maximum thermocline displacement due to the V1H1 wave mode of 23.5 m. yielding a value of $T_{M;VT}$ of ~12 h. For the duration of the experiment, the average excursion from trough to crest height was 15 m for the V1H1 wave mode, with a period of about 24.5 h resulting in a vertical velocity of about 1.25 m h^{-1}. This is far greater than the settling or buoyancy velocities of phytoplankton [*Reynolds*, 2006; *Rigosi et al*., 2011] and suggests that in the metalimnion the phytoplankton could be treated as being passively transported (i.e., frozen flow) such that:

$$\frac{T_{M;VT}}{\tau_M} < 1 < \frac{T_{M;VM}}{\tau_M} \tag{15}$$

Vertical displacements of the peak of metalimnetic biomass generated by basin-scale internal waves determined the depth of the peak biomass in the water column and so the amount of available light (Figure 5a). The scaling thus suggests that phytoplankton residing should be a species that can successfully grow in an environment with low levels of oscillating light and nonturbulent water. It has been observed in several alpine lakes [*Teubner et al*., 2003; *Cuypers et al*., 2011; *Hingsamer et al*., 2014] that the metalimnion provides a refuge for the phytoplankton species (*Planktothrix rubescens*) that also formed the peak concentration in Lake Iseo as seen in Figure 7 (see also *Garibaldi et al*. [2003]). This species usually is present in waters with high TP (Table 1) and low, fluctuating, light-energy [*Watson et al*., 1997; *Reynolds*, 2006] using their gas vesicles inflation mechanism to become neutrally buoyant at the depth of the metalimnion for its optimum low light requirements [*Oberhaus et al*., 2007; *D'Alelio et al*., 2011]. *Diatoma elongatum* is another species that seeks low light levels and relatively low water temperatures [*Sommer*, 1986; *Morabito et al*., 2003; *Busse and Snoeijs*, 2003]. This species assimilates carbon to become neutrally buoyant in water with a density of 998.598 kgm^{-3}. The concentration of TP in the metalimnion was around 21.6 $\mu g\ L^{-1}$ (Table 1), there was an almost total absence of turbulence, and a light availability ranged from 0.1% of the surface light intensity during the internal wave trough to 1% when the crest lifted the chlorophyll *a* maximum to with 10 m of the free surface (Figure 5a).

The well-defined chlorophyll *a* patch, evident along the thalweg of Lake Iseo in Figures 5a and 7a, was either the result of a growth-dispersion balance or a horizontal convergence zone pushing the patch to the south. The temperature (Figure 5) and nutrient levels (Table 1) did not vary much along the length of the

lake [*Leoni et al*., 2014b]. In order to determine the relevant mechanism, the three tracers introduced, one south, one middle, and one north in the grid cell within the thermocline (Figures 8h–8j) along the thalweg of Lake Iseo were used. When averaged over an internal wave period, the simulations showed that no convergence zone forming in the south, the tracer seeming to spread solely by dispersion from the growth center near station P6. The dispersion of the tracers showed an average dispersion coefficient, $\kappa_{M;HM}$, of about 1.7 $m^2\ s^{-1}$ (Figures 8h–8j) leading to a chlorophyll *a* concentration patch scale from equation (13) of ~4.5 km for a growth period of 8 days. This compares well with the chlorophyll *a* concentration patch observed in Figures 5a and 7a, implying a time-scale hierarchy in the metalimnion:

$$\frac{T_{M;VT}}{\tau_M} < 1 < \frac{T_{M;HM}}{\tau_M} < \frac{T_{M;VM}}{\tau_M} \tag{16}$$

Given the small vertical diffusivity in the metalimnion, the origin of the nutrients must be advected into the bulk of the lake horizontally, supported by rectification of the peristaltic action of V2H1 basin-scale internal waves or by a benthic boundary layer intrusion. *Marti and Imberger* [2008] showed, using data from Lake Kinneret, that the V2H1 basin-scale internal wave modes set up a horizontal transport within the metalimnion that can transport material, from the lake boundary to the lake interior with velocities associated with the V2H1 basin-scale internal waves [*Valerio et al*., 2012]. The numerical simulations showed that in Lake Iseo the V2H1 mode supports a longitudinal velocity in the metalimnion of around 0.04 m s^{-1}. From Figure 5a and from *Leoni et al*. [2014b], it is seen that the chlorophyll *a* and nutrient concentrations have a longitudinal scale, L_C, in the metalimnion comparable to that of the quarter length of the lake, around 4.5 km. This implies a horizontal transport time scale $T_{M;HT}$ of around 1.3 days, about the same time as τ_M (Table 2), such that:

$$\frac{T_{M;VT}}{\tau_M} < 1 \sim \frac{T_{M;HT}}{\tau_M} < \frac{T_{M;HM}}{\tau_M} < \frac{T_{M;VM}}{\tau_M} \tag{17}$$

This time-scale hierarchy suggests that the metalimnion forms a growth niche for phytoplankton where nutrient concentrations are maintained by the benthic boundary layer flux, as previously documented in Lake Kinneret by *Marti and Imberger* [2006]; where phytoplankton, once growing, are cycled through a diurnal light regime with peak diurnal intensities equivalent to a water depth of between 5 and 20 m; and where phytoplankton growth is not drained away by dispersion or vertical migration and or sinking. Indeed, vertical dispersion is extremely low and any patch that forms is completely contained within the thermocline and horizontal dispersion spreading is weak enough so as to not drain the phytoplankton concentration for any species with a growth time scale shorter than days to a week. *Planktothrix rubescens* and *Diatoma elongatum* have these attributes, so it is not surprising that these were the dominant species at this depth, sharing the same metalimnion niche [*Garibaldi et al*., 2003; *Morabito et al*., 2003].

4.3. Inflows

The Lake Iseo main inflows are the Oglio River and the Industrial Canal located at the northern shore (Figure 1) and the annual flow rates suggest a bulk residence time of ~4 years [*Pilotti et al*., 2014a]. During the study period, the Industrial Canal had an average discharge of 40 $m^3\ s^{-1}$, average salinity of 0.33 and water temperature varying between 11.3 and 14.9°C, while the Oglio River had an average discharge of 9.8 $m^3\ s^{-1}$, average salinity of 0.13 and water temperatures varying between 11.6 and 19°C. Using salinity measurements and calculations based on the intrusion dynamics, *Hogg et al*. [2013] found that both inflows plunged to depth and then, upon reaching neutral buoyancy, entered the lake as an inflow intrusion between the 18°C and 22°C isotherms, at a depth close to where the chlorophyll *a* maximum was located (see Figure 5a). The horizontal length scale of the inertia-buoyancy intrusion was of the order of 4 km with an inflow time scale, $T_{I;HT}$, of about 1 day similar to both $T_{M;VT}$ and $T_{M;HT}$. This similarity ensures that the intrusion depth continuously adjusts to the depth of the thermocline. Given that

$$T_{M;VT} < T_{I;HT} \sim T_{M;HT} \sim \tau_M < T_{M;HM} < T_{M;VM} \tag{18}$$

the flow is frozen both with respect to the vertical motion due to heaving of the thermocline and with respect to the horizontal flow due to the submerged river intrusions; over the inflow length the phytoplankton would simply reflect the lower chlorophyll *a* concentration found in the inflowing water, hence the

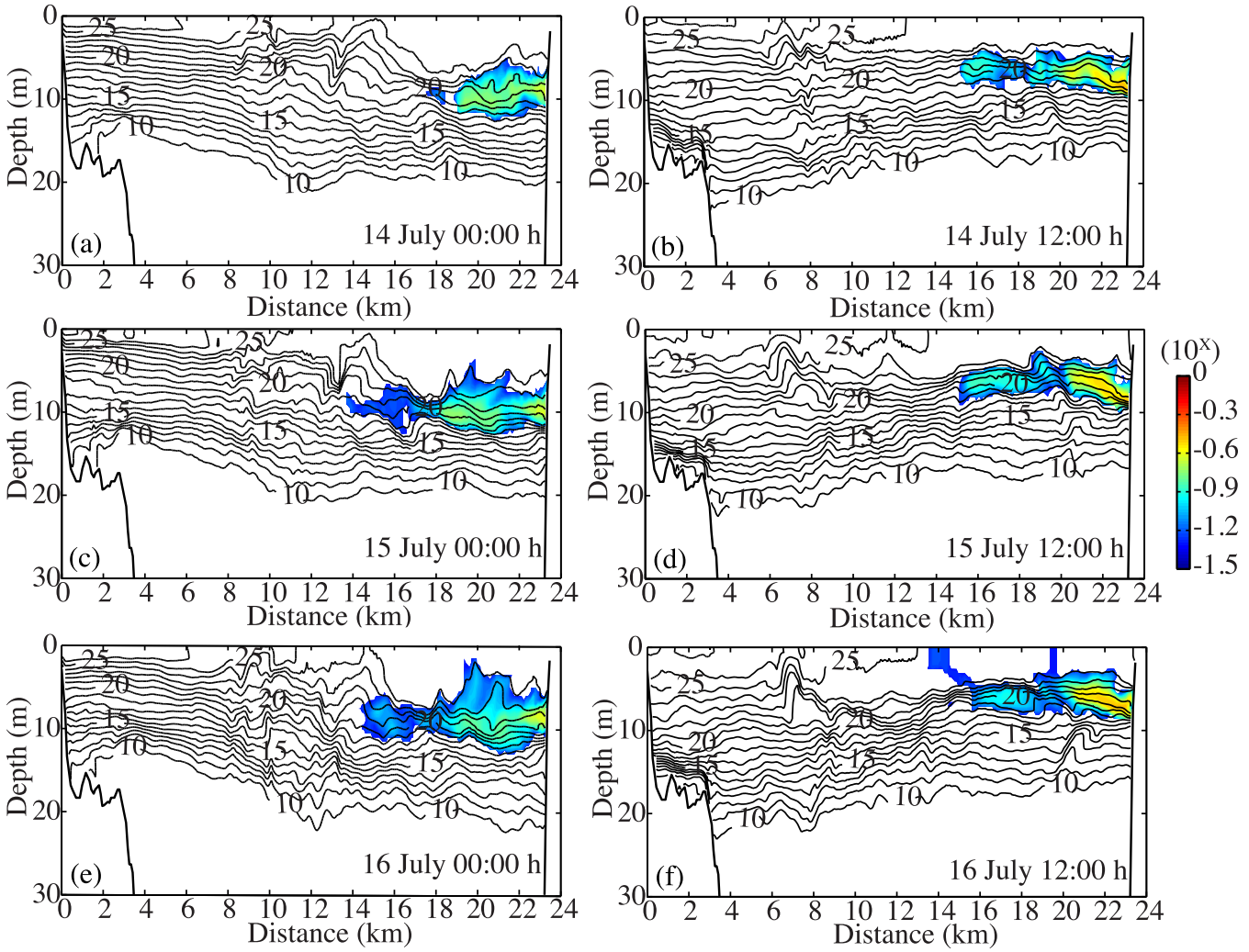

Figure 10. Simulated tracer concentration released in the Industrial Canal along the longitudinal axis (south-north) of the lake at different times during 2 days. Simulated temperature contours are superimposed and shown as solid lines. The bottom isotherm is 10°C and the contour interval is 1°C.

chlorophyll *a* concentrations seen at depth in Figure 5a. These characteristics were also confirmed by simulating a tracer introduced into the Industrial Canal inflow as illustrated in Figure 10.

5. Conclusions

The phytoplankton communities that live in the surface layer and metalimnion of Lake Iseo were observed to possess strong heterogeneity in their vertical variation, but only weak variations were observed horizontally. Using time-scale analysis, it has been possible to determine a clear partition of the time scales of the physical and biological processes in Lake Iseo at the time of the field measurements that explain why the observed species are found where they were. This is similar to what was observed in a tidal salt marsh estuary by *Imberger et al.* [1983] and for a coral reef by *Hatcher et al.* [1987]. In all cases, by establishing the time-scale hierarchy of both the physical and biological processes it has been possible to show the consistency of the observed phytoplankton species and the temporal and spatial characteristics of the phytoplankton patches in Lake Iseo with the known attributes of the species. It has been possible to explain why the cyanobacteria, *Planktothrix rubescens*, and diatoms, *Diatoma elongatum*, were found within the metalimnion because of the peculiar physical and chemical features (high thermal stability, mild light, and nutrient richness) in the establishment of the metalinmetic niche also reported in other alpine lakes [e.g., *Teubner et al.*, 2003; *Morabito et al.*, 2003] and why they were swept ahead on the Industrial Canal submerged intrusion. Similarly, the

hydrodynamics environment as characterized by the associated time-scale hierarchy dictated success of the green algae, *Sphaerocystis schroeterii* found to dominate in the surface layer. Indeed, the time-scale hierarchy mandates the attributes or traits phytoplankton must possess in order to be successful in a particular section of the water column and/or water body. With this work, we demonstrate the importance of using time-scale analysis to develop a general framework to determine the composition of the phytoplankton community in the water column of stratified lakes that is supported by field data. Further, it provides as a useful tool for designing field studies that characterize the physical and biological processes and appropriate measures of system response for understating water quality variability.

Acknowledgments
The authors acknowledge the financial support of the **Australian Research Council Discovery** Project DP1096728 and **Università degli Studi di Milano-Bicocca** (**FAR 2009**). Investigations in Lake Iseo were made in the framework of the LTER (Long Term Ecological Research) Italian network, site "Southern Alpine lakes," IT08-000-A (http://www.lteritalia.it/). The personnel of the Centre for Water Research are thanked, in particular Gregory Attwater, Lee Goodyear, Roger Head, Carol Lam, and Angus Steward for their support on the acquisition of field data during the experiment in Lake Iseo. The model used in this study, ELCOM, is available for an annual fee through the Zephyr systems web site (http://zephyr.science.uwa.edu.au/). Field data and input files necessary to reproduce the model results with ELCOM are available from the authors upon request (marti1clelia@gmail.com). We thank the reviewers and the editor for their insightful comments. This article forms Centre for Water Research reference 2483-CM.

References

APHA, AWWA, and WEF (1995), *Standard Methods for the Examination of Water and Wastewater*, 19th ed., 43 pp., Am. Publ. Health Assoc., Washington, D. C.

Atkinson, M. J., T. Berman, B. R. Allanson, and J. Imberger (1987), Fine-scale oxygen variability in a stratified estuary: Patchiness in aquatic environments, *Mar. Ecol. Prog. Ser.*, *36*, 1–10.

Blenckner, T., et al. (2007), Large-scale climatic signatures in lakes across Europe: A meta-analysis, *Global Change Biol.*, *13*, 1314–1326.

Boehrer, B., and M. Schultze (2008), Stratification of lakes, *Rev. Geophys.*, *46*, RG2005, doi:10.1029/2006RG000210.

Bright, D. I., and A. E. Walsby (2000), The daily integral of growth by *Planktothrix rubescens* calculated from growth rate in culture and irradiance in Lake Zürich, *New Phytol.*, *146*, 301–316.

Busse, S., and P. Snoeijs (2003), Gradient responses of diatom communities in the Bothnian Sea (northern Baltic Sea), with emphasis on responses to water movement, *Phycologia*, *42*(5), 451–464.

Cuypers, Y., B. Vinçon-Leite, A. Groleau, B. Tassin, and J. Humbert (2011), Impact of internal waves on the spatial distribution of *Planktothrix rubescens* (cyanobacteria) in an alpine lake, *ISME J.*, *5*, 580–589.

D'Alelio, D., A. Gandolfi, A. Boscaini, G. Flaim, M. Tolotti, and N. Salmaso (2011), *Planktothrix* populations in subalpine lakes: Selection for strains with strong gas vesicles as a function of lake depth, morphometry and circulation, *Freshwater Biol.*, *56*, 1481–1493.

Denman, K. L., and A. E. Gargett (1983), Time and space scales of vertical mixing and advection of phytoplankton in the upper ocean, *Limnol. Oceanogr.*, *28*(5), 801–815.

Denman, K. L., and T. M. Powell (1984), Effects of physical processes on planktonic ecosystems in the coastal ocean, *Oceanogr. Mar. Biol. Ann. Rev.*, *22*, 125–168.

Durham, W. M., E. Climent, M. Barry, F. De Lillo, G. Boffetta, M. Cencini, and R. Stocker (2013), Turbulence drives microscale patches of motile phytoplankton, *Nat. Commun.*, *4*(2148), doi:10.1038/ncomms3148.

Eckert, W., J. Imberger, and A. Saggio (2002), Biogeochemical response to physical forcing in the water column of a warm monomictic lake, *Biogeochemistry*, *61*(3), 291–307, doi:10.1023/A:1020206511720.

Evans M. A., S. MacIntyre, and G. W. Kling (2008), Internal wave effects on photosynthesis: Experiments, theory, and modeling. *Limnol. Oceanogr*, *53*, 339–353, doi:10.4319/lo.2008.53.1.0339.

Fischer, H. B., E. J. List, R. C. Y. Koh, J. Imberger, and N. H. Brooks (1979), *Mixing in Inland and Coastal Waters*, 483 pp., Acad. Press, N. Y.

Fozdar, F. M., G. J. Parker, and J. Imberger (1985), Matching temperature and conductivity sensor response characteristics, *J. Phys. Oceanogr.*, *15*(11), 1557–1569.

Gallina, N., N. Salmaso, G. Morabito, and M. Beniston (2013), Phytoplankton configuration in six deep lakes in the peri-Alpine region: Are the key drivers related to eutrophication and climate?, *Aquat. Ecol.*, *47*, 177–193, doi:10.1007/s10452-013-9433-4.

Garibaldi, L., V. Mezzanotte, M. C. Brizzio, M. Rogora, and R. Mosello (1999), The trophic evolution of Lake Iseo as related to its holomixis, *J. Limnol.*, *58*(1), 10–19.

Garibaldi, L., A. Anzani, A. Marieni, B. Leoni, and R. Mosello (2003), Studies on the phytoplankton of the deep subalpine Lake Iseo, *J. Limnol.*, *62*(2), 177–189.

George, D. G., and S. I. Heaney (1978), Factors influencing the spatial distribution of phytoplankton in a small productive lake, *J. Ecol.*, *66*, 135–155.

Harris, G. P., and A. M. Trimbee (1986), Phytoplankton population dynamics of a small reservoir: Physical/biological coupling and the time scales of community change, *J. Plankton Res.*, *8*, 1011–1025.

Hatcher, B. G., J. Imberger, and S. V. Smith (1987), Scaling analysis of coral reef systems: An approach to problems of scale, *Coral Reefs*, *5*, 171–181.

Hingsamer, P., F. Peeters, and H. Hofmann (2014), The consequences of internal waves for phytoplankton focusing on the distribution and production of *Planktothrix rubescens*, *PLoS One*, *9*(8), e104359, doi:10.1371/journal.pone.0104359.

Hodges, B., J. Imberger, A. Saggio, and K. Winters (2000), Modeling basin-scale internal waves in a stratified lake, *Limnol. Oceanogr.*, *45*, 1603–1620.

Hogg, C. A. R., C. L. Marti, H. E. Huppert, and J. Imberger (2013), Mixing of an interflow into the ambient water of Lake Iseo, *Limnol. Oceanogr.*, *58*(2), 579–592.

Imberger, J. (1977), On the validity of water quality models for lakes and reservoirs, paper presented at 17th International Association for Hydro-Environment Engineering and Research World Congress, IAHR, Baden, Germany.

Imberger, J. (1985), The diurnal mixed layer, *Limnol. Oceanogr.*, *30*(4), 737–770.

Imberger, J. (1994) Transport processes in lakes: A review article, in *Limnology Now: A Paradigm of Planetary Problems*, edited by R. Margalef, pp. 99–193, Elsevier Sci., Amsterdam.

Imberger, J. (2013), *Environmental Fluid Dynamics*, 430 pp., Acad. Press, San Diego, Calif.

Imberger, J., T. Berman, R. R. Christian, E. B. Sherr, D. E. Whitney, L. R. Pomeroy, R. G. Wieger, and W. J. Wiebe (1983), The influence of water motion on the distribution and transport of materials in a salt marsh estuary, *Limnol. Oceanogr.*, *28*(2), 201–214.

Kampe H., M. König-Rinkeb, T. Petzoldt, and J. Benndorf (2007), Direct effects of *Daphnia*-grazing, not infochemicals, mediate a shift towards large inedible colonies of the gelatinous green alga *Sphaerocystis schroeteri*, *Limnologica*, *37*, 137–145, doi:10.1016/j.limno.2007.01.001.

Kierstead, H., and L. B. Slobodkin (1953), The size of water masses containing plankton blooms, *J. Mar. Res.*, *12*(1), 141–147.

Kling, G. W., M. A. Clark, G. N. Wagner, H. R. Compton, A. M. Humphrey, J. D. Devine, W. C. Evans, J. P. Lockwood, M. L. Tuttle, and E. J. Koenigsberg (1987), The 1986 Lake Nyos Gas Disaster in Cameron, West Africa, *Science*, *236*(4798), 169–175.

Koseff, J., J. Holen, S. Monismith, and J. Cloern (1993), Coupled effects of vertical mixing and benthic grazing on phytoplankton populations in shallow, turbid estuaries, *J. Mar. Res.*, *51*, 843–868.
Laval, B., J. Imberger, B. R. Hodges, and R. Stocker (2003), Modelling circulation in lakes: Spatial and temporal variations, *Limnol. Oceanogr.*, *48*(3), 983–994.
Lawrence, G. A., K. I. Ashley, N. Yonemitsu, and J. R. Ellis (1995), Natural dispersion in a small lake, *Limnol. Oceanogr.*, *40*(8), 1519–1526.
Leoni, B., L. Garibaldi, and R. Gulati (2014a), How does interannual trophic variability caused by vertical water mixing affect reproduction and population density of the Daphnia longispina group in Lake Iseo, a deep stratified lake in Italy?, *Inland Waters*, *4*(2), 193–203.
Leoni, B., C. L. Marti, J. Imberger, and L. Garibaldi (2014b), Summer spatial variations in phytoplankton composition and biomass in surface waters of a warm-temperate, deep, oligo-holomitic lake: Lake Iseo, Italy, *Inland Waters*, *4*(3), 303–310.
Lund, J. W. G., C. Kipling, and E. D. Le Cren (1958), The Inverted Microscope method of estimating algal numbers and the statistical basis of estimations by counting, *Hydrobiologia*, *11*, 143–170.
Machado, D. A., C. L. Marti, and J. Imberger (2014), Influence of microscale turbulence on the phytoplankton of a temperate coastal embayment, *Estuarine Coastal Shelf Sci.*, *145*, 80–95.
McCabe, S. K., and H. Cyr (2006), Environmental variability influences the structure of benthic algal communities in an oligotrophic lake, *Oikos*, *115*,197–206.
Marti, C. L., and J. Imberger (2006), Dynamics of the benthic boundary layer in a strongly forced stratified lake. *Hydrobiologia*, *568*(1), 217–233.
Marti, C. L., and J. Imberger (2008), Exchange between littoral and pelagic waters due to wind induced motions in a stratified lake: Lake Kinneret, Israel. *Hydrobiologia*, *603*(1), 25–51.
Marti, C. L., R. Mills, and J. Imberger (2011), Mechanisms influencing the mixing and transport of multiple inflows into a stratified reservoir: Thomson Reservoir; Australia, *Adv. Water Resour.*, *34*(5), 551–561.
McDougall, T. J. (1978), Bubble Plumes In Stratified Environments, *J. Fluid Mech.*, *85*, 655–672.
Michalak, A. M., et al. (2013), Record-setting algal bloom in Lake Erie caused by agricultural and meteorological trends consistent with expected future conditions, *Proc. Natl. Acad. Sci. U. S. A.*, *110*, 6448–6452.
Morillo, S., J. Imberger, J. Antenucci, and D. Copetti (2009), Using impellers to distribute local nutrient loadings in a stratified lake: Lake Como, Italy, *J. Hydraul. Eng.*, *135*(7), 564–574.
Morabito, G., A. Oggioni, and P. Panzani (2003), Phytoplankton assemblage at equilibrium in large and deep subalpine lakes: A case study from Lago Maggiore (N. Italy), *Hydrobiologia*, *502*, 37–48.
Nishri, A., J. Imberger, W. Eckert, I., Ostrowski, and Y. Geifman (2000), The physical regime and the respective biogeochemical processes in the lower water mass of Lake Kinneret, *Limnol. Oceanogr.*, *45*, 972–981.
Oberhaus, L., Briand, J. F., Leboulanger, C., Jacquet, S., and J. F. Humbert (2007), Comparative effects of the quality and quantity of light and of temperature on the growth of *Planktothrix agardhii* and *P. rubescens*, *J. Phycol.*, *43*, 1191–1199.
Okubo, A. (1971), Oceanic diffusion diagrams, *Deep Sea Res. Oceanogr. Abstr.*, *18*, 789–802.
Pilotti, M., G. Valerio, and B., Leoni (2013), Data set for hydrodynamic lake model calibration: A deep pre-alpine case, *Water Resour. Res.*, *49*, 7159–7163, doi:10.1002/wrcr.20506.
Pilotti, M., S. Simoncelli, and G. Valerio (2014a), A simple approach to the evaluation of the actual water renewal time of natural stratified lakes, *Water Resour. Res.*, *50*, 2830–2849, doi:10.1002/2013WR014471.
Pilotti, M., G. Valerio, L. Gregorini, L. Milanesi, and C. Hogg (2014b), Study of tributary inflows in lake Iseo with a rotating physical model, *J. Limnol.*, *73*(1), 131–145, doi:10.4081/jlimnol.2014.772.
Reynolds, C. S. (2006), *Ecology of Phytoplankton*, 535 pp., Cambridge Univ. Press. N. Y.
Richardson, K., J. Beardall, and J. A. Raven (1983), Adaptation of unicellular algae to irradiance: An analysis of strategies, *New Phytol.*, *93*, 157–191.
Rigosi, A., R. Marce, C. Escot, and F. Rueda (2011), A calibration strategy for dynamic succession models including several phytoplankton groups, *Environ. Modell. Software*, *26*, 697–710.
Rott, E., N. Salmaso, and E. Hoehn (2007), Quality control of Utermöhl based phytoplankton biovolume estimates - an easy task or a Gordian knot? *Hydrobiologia*, *578*, 141–146.
Saggio, A., and J. Imberger (1998), Internal wave weather in a stratified lake, *Limnol. Oceanogr.*, *43*(8), 1780–1795.
Salmaso, N., G. Morabito, R. Mosello, L. Garibaldi, M. Simona, F. Buzzi, and D. Ruggi (2003), A synoptic study of phytoplankton in the deep lakes south of the Alps (lakes Garda, Iseo, Como, Lugano and Maggiore), *J. Limnol.*, *62*(2), 207–227.
Schindler, D. W., R. E. Hecky, and G. K. McCullough (2012), The rapid eutrophication of Lake Winnipeg: Greening under global change, *J. Great Lakes Res.*, *38*, suppl. 3, 6–13.
Silva, C. P., C. L. Marti, and J. Imberger (2014), Physical and biological controls of algal blooms in the Rio de la Plata, *Environ. Fluid Mech.*, *14*(5), 1–30, doi:10.1007/s10652-014-9342-7.
Sommer, U. (1986), The periodicity of phytoplankton in Lake Constance (Bodensee) in comparison to other deep lakes of central Europe, *Hydrobiologia*, *138*, 1–7.
Teubner, K., M. Tolotti, S. Greisberger, H. Morscheid, M. T. Dokulil, and H. Morscheid (2003), Steady state phytoplankton in a deep prealpine lake: Species and pigments of epilimnetic versus metalimetic assemblages, *Hydrobiologia*, *502*, 49–64.
Trolle, D., et al. (2012), A community-based framework for aquatic ecosystem models, *Hydrobiologia*, *683*(1), 25–34, doi:10.1007/s10750-011-0957-0.
Valerio, G., M. Pilotti, C. L. Marti, and J. Imberger (2012), The structure of basin scale internal waves in a stratified lake in response to lake bathymetry and wind spatial and temporal distribution: Lake Iseo, Italy, *Limnol. Oceanogr.*, *57*, 772–786.
Valerio, G., M. Pilotti, S. Barontini, and B. Leoni (2015), Sensitivity of the multiannual thermal dynamics of a deep pre-alpine lake to climate change, *Hydrol. Processes*, *29*(5), 767–779.
Vidal, J., A. Rigosi, A. Hoyer, C. Escot, and F. J. Rueda (2014), Spatial distribution of phytoplankton cells in small elongated lakes subject to weak diurnal wind forcing, *Aquat. Sci.*, *76*, 83–99.
Vilhena L. C., C. L. Marti, and J. Imberger (2013), The importance of nonlinear internal waves in a deep sub-alpine lake: Lake Iseo, *Limnol. Oceanogr.*, *58*(5), 1871–1891.
Verburg, P., and R. E. Hecky (2009), The physics of the warming of Lake Tanganyika by climate change, *Limnol. Oceanogr.*, *54*, 2418–2430.
Watson, S. B., E. McCauley, and J. A. Downing (1997), Patterns in phytoplankton taxonomic composition across temperate lakes of differing nutrient status, *Limnol. Oceanogr.*, *42*, 487–495.
Yeates, P. S., A. Gomez-Giraldo, and J. Imberger (2013), Observed relationships between microstructure patches and the gradient Richardson number in a thermally stratified lake, *Environ. Fluid Mech.*, *13*(65), 205–226.